



ARTICLE

DOI: 10.1038/s41467-018-03239-3

OPEN

# The elusive abnormal CO<sub>2</sub> insertion enabled by metal-ligand cooperative photochemical selectivity inversion

Felix Schneck<sup>1</sup>, Jennifer Ahrens<sup>2</sup>, Markus Finger<sup>1</sup>, A. Claudia Stückl<sup>1</sup>, Christian Würtele<sup>1</sup>, Dirk Schwarzer<sup>2</sup> <sup>2</sup> & Sven Schneider<sup>1</sup> 

Direct hydrogenation of CO<sub>2</sub> to CO, the reverse water-gas shift reaction, is an attractive route to CO<sub>2</sub> utilization. However, the use of molecular catalysts is impeded by the general reactivity of metal hydrides with CO<sub>2</sub>. Insertion into M-H bonds results in formates (MO(O)CH), whereas the abnormal insertion to the hydroxycarbonyl isomer (MC(O)OH), which is the key intermediate for CO-selective catalysis, has never been directly observed. We here report that the selectivity of CO<sub>2</sub> insertion into a Ni-H bond can be inverted from normal to abnormal insertion upon switching from thermal to photochemical conditions. Mechanistic examination for abnormal insertion indicates photochemical N-H reductive elimination as the pivotal step that leads to an umpolung of the hydride ligand. This study conceptually introduces metal-ligand cooperation for selectivity control in photochemical transformations.

<sup>1</sup>Universität Göttingen, Institut für Anorganische Chemie, Tammannstr. 4, 37077 Göttingen, Germany. <sup>2</sup>Department of Dynamics at Surfaces, Max Planck Institute for Biophysical Chemistry, Am Fassberg 11, 37077 Göttingen, Germany. Correspondence and requests for materials should be addressed to S.S. (email: [sven.schneider@chemie.uni-goettingen.de](mailto:sven.schneider@chemie.uni-goettingen.de))

Selectivity control is a key issue for CO<sub>2</sub> functionalization to added value products. The products from CO<sub>2</sub> reduction can range from oxalic acid (1-electron) to carbon monoxide or formic acid (2-electron), formaldehyde (4-electron), and methanol (6-electron) all the way to hydrocarbons<sup>1</sup>. The primary industrial C<sub>1</sub> building block CO is a particularly attractive target. In nature, CO<sub>2</sub> reduction to CO is catalyzed by the enzyme [NiFe] carbon monoxide dehydrogenase ([NiFe]-CODH), which contains a nickel capped [Fe<sub>4</sub>S<sub>4</sub>Ni]-cluster as active site<sup>1</sup>. The proposed mechanism comprises CO<sub>2</sub> binding to nickel followed by formation of a hydroxycarbonyl bridged {Ni(CO<sub>2</sub>H)Fe} intermediate as selectivity deriving step upon electron and proton transfer. Alternatively, CO<sub>2</sub> insertion into a Ni–H bond has also been discussed<sup>2</sup>. In analogy, metalcarboxylate (MCO<sub>2</sub>H/M) species are also proposed as the key intermediates for synthetic CO-selective molecular catalysis, yet rarely detected<sup>3–8</sup>. Such systems are generally electro- or photochemically driven<sup>1,9–12</sup> as direct hydrogenation by reverse water–gas shift (RWGS) is endothermic (see equation 1).

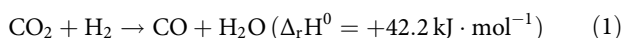
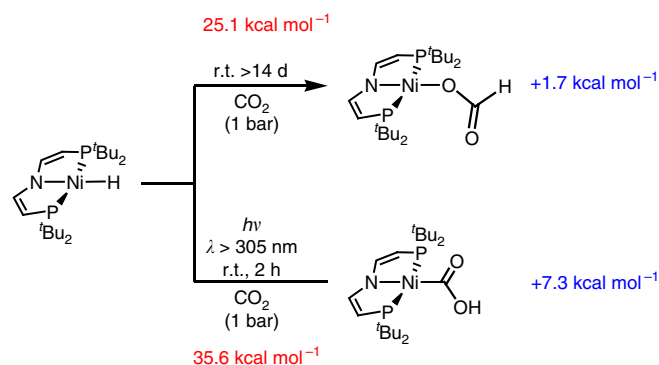


Photo-driven direct RWGS would be a highly desirable alternative to (photo)electrocatalysis. But this route also faces a major kinetic challenge, which disfavors CO formation: CO<sub>2</sub> hydrogenation via molecular hydride catalysts generally leads to formic acid (or methanol) instead of CO<sup>13–16</sup>. This selectivity is a consequence of the normal CO<sub>2</sub> insertion into M–H bonds giving formates (MO<sub>2</sub>CH)<sup>17</sup>. In contrast, the alternative formation of the hydroxycarbonyl (MCO<sub>2</sub>H) isomer has never been directly observed and is therefore referred to as abnormal CO<sub>2</sub> insertion<sup>13</sup>.

Nickel pincer complexes were recently studied both as [NiFe]-CODH models and in catalytic CO<sub>2</sub> hydrogenation to formate<sup>18–21</sup>. Inspired by the biological and synthetic precedence, we here report the photo-driven inversion of the CO<sub>2</sub> insertion selectivity into a Ni–H bond representing an example of abnormal CO<sub>2</sub> insertion. The selectivity is defined by photoinduced *trans* N–H reductive elimination as an application of metal–ligand cooperativity in photocatalysis.

## Results

**Thermal vs. photochemical CO<sub>2</sub> insertion.** Nickel(II) hydride complex [NiH(PNP)] (**1**, PNP = N(CHCHP*t*Bu<sub>2</sub>)<sub>2</sub>) can be prepared from the previously reported bromide [NiBr(PNP)] with LiAlH<sub>4</sub><sup>22</sup>. As expected, the reaction of **1** with CO<sub>2</sub> (1–10 bar) at room temperature (r.t.) gives formate complex [Ni(O<sub>2</sub>CH)(PNP)] (**2**, Fig. 1) as the product of normal insertion. However, the reaction is sluggish and takes several days for completion even at *p*(CO<sub>2</sub>) = 10 bar. In contrast to this thermal reactivity, bulk photolysis of **1** ( $\lambda_{\text{exc}} > 305 \text{ nm}$ , Supplementary Fig. 15) in benzene or THF under CO<sub>2</sub> (1 bar) at r.t. results in full conversion of **1** within a few hours (Fig. 1). A quantum yield around  $\Phi_p = 5\%$  was estimated actinometrically using a ferrioxalate assay (Supplementary Fig. 37). Importantly, the abnormal insertion product [Ni<sup>II</sup>(CO<sub>2</sub>H)(PNP)] (**3**) is formed as the main product in ~70% spectroscopic and isolated yield with no indication for formate **2**. In the solid state, the bond metrics of the {NiCO<sub>2</sub>H} entity (Fig. 2) resemble the other previously reported nickel hydroxycarbonyl complex, which was not obtained directly from CO<sub>2</sub><sup>18</sup>. Besides **3**, small amounts (ca. 20%) of the hydrocarbonate complex [Ni(OCO<sub>2</sub>H)(PNP)] (**4**, Fig. 2) and trace quantities of nickel(I) complex [Ni(CO)(PNP)] (**5**, Fig. 2) are observed by nuclear magnetic resonance (NMR) and electron paramagnetic resonance (EPR) spectroscopy (Supplementary Figs. 28, 29), respectively, as the only side products. Kinetic monitoring of the



**Fig. 1** Experimental conditions for normal vs. abnormal CO<sub>2</sub> insertion. Reactivity of **1** with CO<sub>2</sub> under thermal and photochemical conditions, respectively, with computed (D3(BJ)-RI-J-PBE/def2-SVP//D3(BJ)-TPSS/def2-TZVP(Cosmo:THF)) free reaction enthalpies ( $\Delta_r G^0$ (298 K), blue) and effective reaction barriers ( $\Delta G_{\text{eff}}^\ddagger$ (298 K) red) for the respective thermal insertions

photolysis (Fig. 3a) indicates slow underlying conversion of **3** to **4** by CO extrusion and CO<sub>2</sub> insertion as the source of hydrocarbonate and carbonyl side products. Accordingly, photolysis of isolated **3** under argon gives the hydroxy complex [Ni(OH)(PNP)] (**6**, Fig. 2) in high yield within competitive timescales and **6** selectively inserts CO<sub>2</sub> to hydrocarbonate **4** (Fig. 4a, Supplementary Fig. 16).

**Mechanistic examinations.** In agreement with the experimental findings, thermal normal insertion was computed to be slow and strongly favored over endergonic abnormal insertion both thermodynamically and kinetically (Fig. 1). Mechanistic examinations were conducted to rationalize this photochemical selectivity inversion. Photolysis of the [NiD(PNP)] isotopologue under CO<sub>2</sub> results in almost quantitative transfer of the deuterium label to the hydroxy proton of **3**, thus confirming the hydride ligand as the primary hydrogen source (Supplementary Fig. 25). The reaction rate exhibits first-order dependence in **1** and photon flux, respectively, but is independent from CO<sub>2</sub> pressure between 1 and 10 bar (Supplementary Figs. 20–25). Therefore, the photochemistry of **1** in the absence of CO<sub>2</sub> was first studied. Hydride H/D exchange with TEMPO-D (2,2,6,6-tetramethylpiperidinyldeteroxide; 10 equiv.) is observed only under photolytic conditions (Supplementary Fig. 19). In contrast, H/D scrambling with *t*BuOD is obtained neither in the dark nor upon photolysis, suggesting homolytic rather than heterolytic Ni–H photoactivation. Accordingly, photolysis of **1** in benzene or THF under argon (Fig. 4b) gives [Ni(PNP)] (**7**) as the only detectable product by NMR and EPR spectroscopy upon comparison with an analytically pure sample prepared by reduction of [NiBr(PNP)] with Mg (Supplementary Figs. 17 and 30). Liberation of H<sub>2</sub> was confirmed by gas chromatography headspace analysis (Supplementary Fig. 18). The rhombic *g*-tensor ( $g_x = 2.29$ ,  $g_y = 2.25$ ,  $g_z = 2.01$ ) and <sup>14</sup>N superhyperfine interaction ( $A_z = 34 \text{ MHz}$ ) of **7** are in agreement with nickel(I) and some spin delocalization onto the pincer ligand, which is confirmed by density functional theory (DFT) computations ( $\rho_{\text{Ni}} = 91\%$ ; Supplementary Fig. 42). In analogy to other nickel(I) complexes with similar spectroscopic features<sup>20,23,24,25</sup>, the molecular structure of **7** (Fig. 2) reveals T-shaped nickel coordination.

The observation of the photoreduction products **7** and **5** raises the question about the role of nickel(I) for abnormal insertion, e.g. via a radical chain mechanism. **7** reacts with equimolar amounts of CO<sub>2</sub> in the dark and under photochemical conditions to one diamagnetic compound (Fig. 4b). NMR spectroscopic

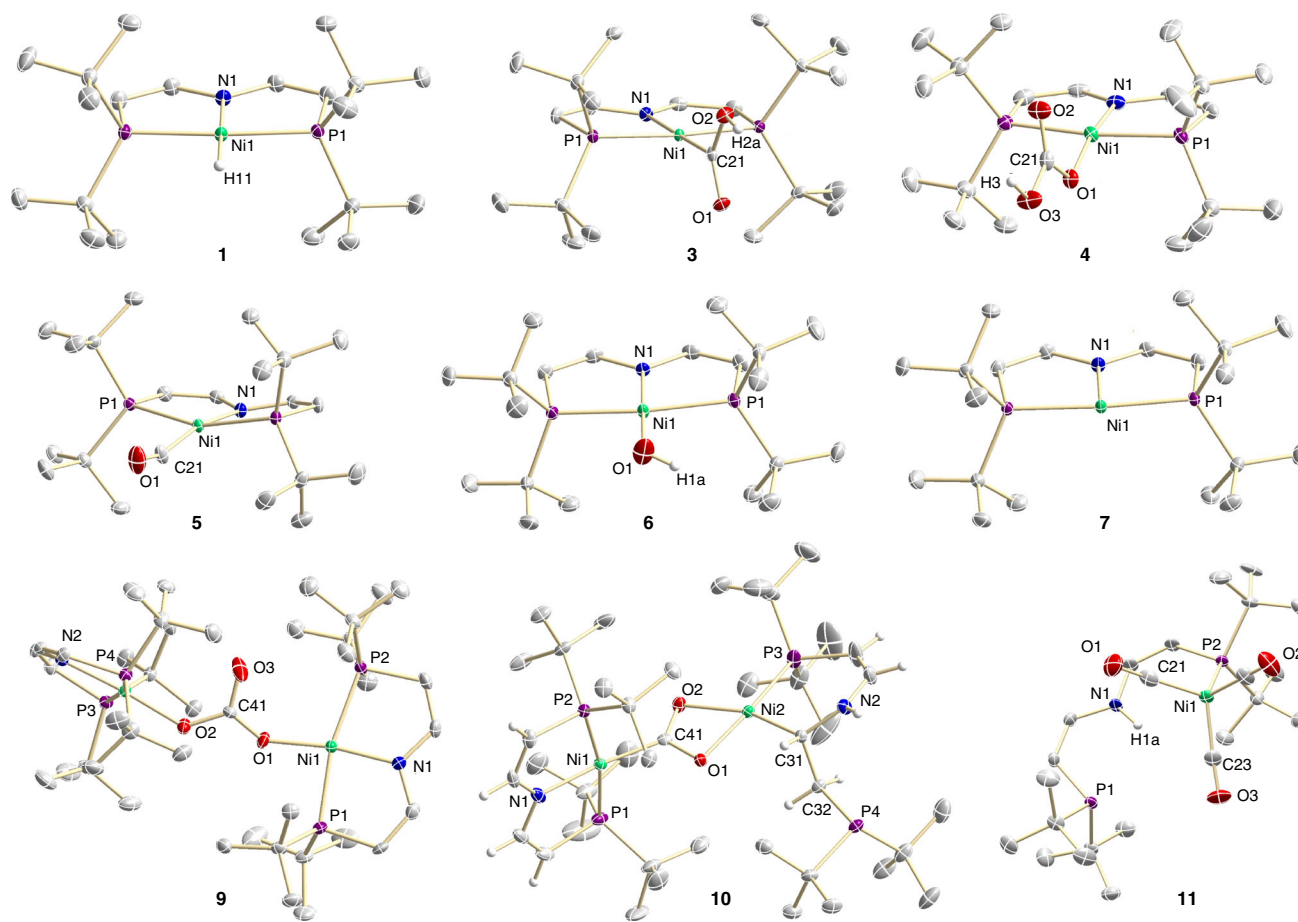


**Fig. 2** Molecular structures of nickel compounds relevant to CO<sub>2</sub> activation. Structures of **1**, **3–7**, and **9–11** in the solid state derived by single-crystal X-ray diffraction. For crystallographic details see Supplementary Figs. 48–56 and Supplementary Tables 19–47

characterization of the <sup>13</sup>CO<sub>2</sub> isotopologue is in agreement with the formation of a dinuclear CO<sub>2</sub>-bridged ( $\delta(^{13}\text{C}) = 237$  ppm) Ni<sup>II</sup>/Ni<sup>II</sup> complex, in analogy with a related nickel(I) pincer complex<sup>20</sup>. In the current case, the product [(PNP)Ni<sup>II</sup>(1 $\kappa^2$ C,2 $\kappa^2$ O, O'-CO<sub>2</sub>)Ni<sup>II</sup>( $\kappa^2$ P,N-PNP)] (**8**) bears one tridentate ( $\delta(^{31}\text{P}) = 67.8$  ppm) and one bidentate pincer ligand ( $\delta(^{31}\text{P}) = 72.2$  and 4.8 ppm), respectively, presumably as a consequence of increased steric pressure. At 1 bar CO<sub>2</sub>, **8** subsequently eliminates CO and inserts CO<sub>2</sub> (Fig. 4b) to the dinuclear carbonate bridged complex [(PNP)Ni<sup>II</sup>(OC(O)O)Ni<sup>II</sup>(PNP)] (**9**, Fig. 2). In the presence of **1** (without irradiation) this reactivity of **7** with CO<sub>2</sub> remains unchanged. Importantly, **1** is not consumed under these conditions disfavoring a radical chain mechanism for abnormal insertion with photochemically produced **7** as chain propagator. Photolysis of mixtures of **1** and **7** ( $[7]_0 = 0\text{--}1.3 [1]_0$ ) under CO<sub>2</sub> (1 bar) gives rising amounts of binuclear (**9**) vs. mononuclear (**3**) products with increasing  $[7]_0$  (Fig. 3b). In fact, the consumption of **1** even slows with increasing  $[7]_0$ . This rate retardation and the diverging selectivities strongly suggest that nickel(I) complex **7** is not an intermediate in abnormal CO<sub>2</sub> insertion.

**Time-resolved spectroscopy.** Transient spectroscopy was employed to further rationalize the photochemistry of **1**. Pump-probe IR-spectroscopy ( $\lambda_{\text{exc}} = 400$  nm, THF) reveals an instantaneous bleach of the Ni–H stretching vibration at 1845 cm<sup>-1</sup> and simultaneous shift of vibrational modes of the vinylic PNP ligand backbone  $\sim 1500\text{--}1520$  cm<sup>-1</sup> (Fig. 3c–e). The absence of other transient signals within the experimental window (1260–1900 cm<sup>-1</sup>) for both Ni–H/D isotopomers is consistent with the

population of a dissociative state or at least strong weakening of the metal-hydride bond upon excitation (Supplementary Figs. 32, 33, 35). Ground state repopulation can be modeled with a biexponential fit. The immediately formed excited state shows a lifetime of  $\tau_1 = 1.3$  ps. The timescale of the subsequent spectral evolution ( $\tau_2 = 12$  ps) is consistent with vibrational cooling in the electronic ground state of **1**. Although full relaxation is observed for the IR spectrum, transient UV/Vis spectroscopy (Fig. 3f–h, Supplementary Fig. 34;  $\lambda_{\text{exc}} = 400$  nm, THF) reveals the evolution of a band at around 450 nm within the same timescale ( $\tau_2 \approx 13$  ps) that is persistent on the timescale of the pump-probe experiment ( $\tau_3 \gg 1$  ns) and does not originate from nickel(I) complex **7** (Supplementary Fig. 31). The absence of IR-bands assignable to this product is attributed to low quantum yields (<5%). Notably, a weak feature at 450 nm is also observed in the stationary UV/Vis spectrum after bulk photolysis of **1** (Supplementary Fig. 31). Importantly, the rapid rate of all photoprocesses well below the timescale of diffusion exclude bimolecular reactivity of an excited state of **1** with CO<sub>2</sub>, which is in line with the rate independence of abnormal insertion from *p*(CO<sub>2</sub>). Instead, **1** apparently forms a photoproduct with low quantum yield that presumably is a common intermediate for photoreduction to **7** or, alternatively, abnormal insertion in the presence of CO<sub>2</sub>.

**Trapping experiments.** The timescales of the photoprocesses and the retention of the Ni–D label upon reaction with CO<sub>2</sub> support an intramolecular rearrangement to the photoproduct, yet not to nickel(I) as suggested by the kinetics. Further information about the photointermediate was obtained from

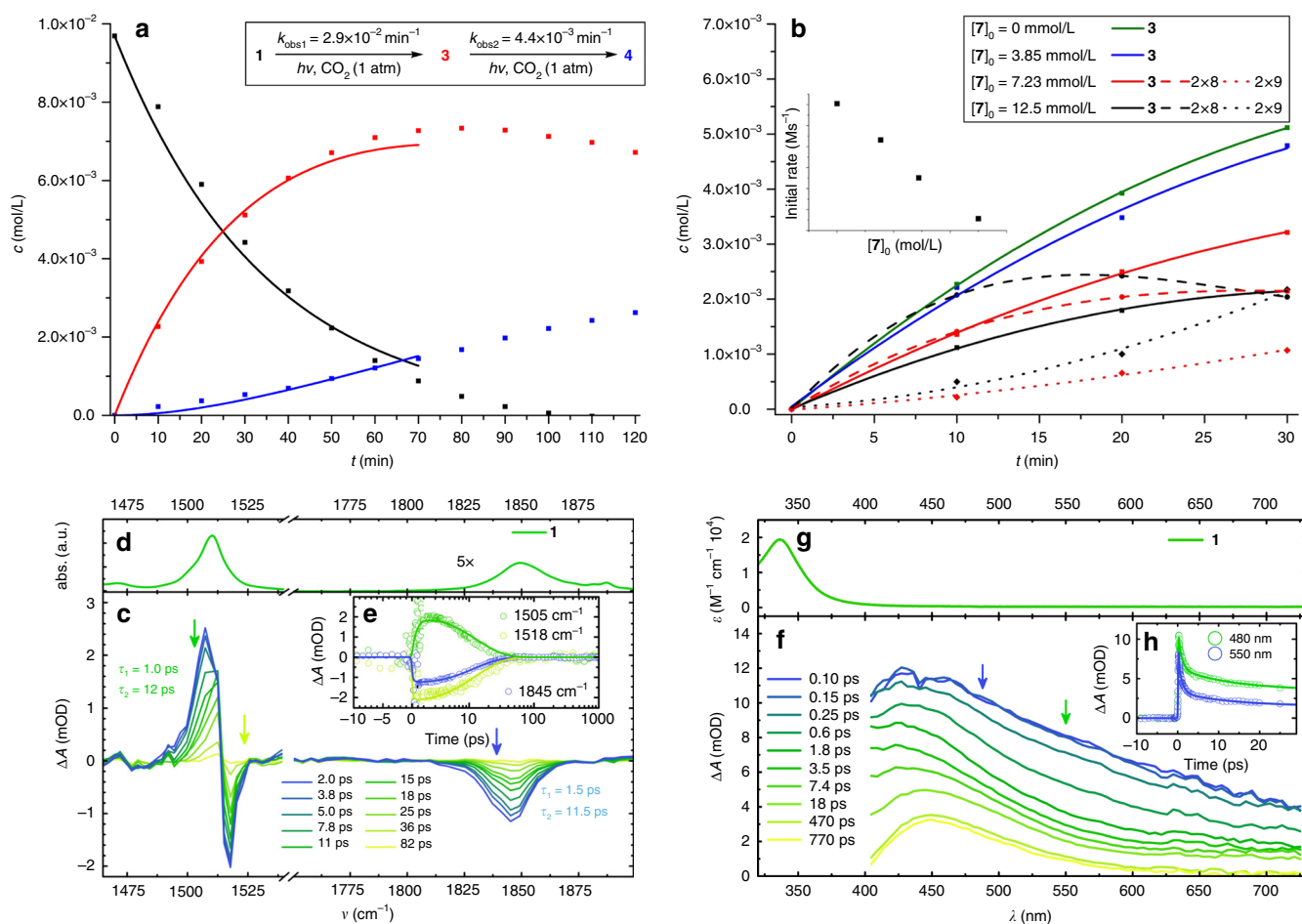


**Fig. 3** Selected kinetic and spectroscopic data. **a** Kinetic data for bulk photolysis of **1** ( $\lambda > 305$  nm,  $[7]_0 = 0$ , THF) and global fit over three half-lives of **1** (solid lines). **b** Initial kinetic data for bulk photolysis of **1** ( $\lambda > 305$  nm, THF) with varying amounts of added **7** (lines are polynomial splines as guide for the eye). **c** Transient IR difference spectra generated by 400 nm excitation of a 11 mM solution of **1** in THF- $d_8$  (1750–1900  $cm^{-1}$ ) and THF (1470–1540  $cm^{-1}$ ), respectively, for selected pump-probe delays. **d** Stationary FTIR spectrum of **1** in THF- $d_8$ . **e** Time traces with biexponential fits (time constants:  $\tau_1 = 1.3 \pm 0.2$  ps,  $\tau_2 = 12 \pm 0.5$  ps). **f** Transient UV/Vis difference spectra generated by 385 nm excitation of a 6 mM solution of **1** in THF for selected pump-probe delays. **g** Stationary absorption spectrum of **1** in THF. **h** Time traces with triexponential fits (time constants:  $\tau_1 = 0.9 \pm 0.2$  ps,  $\tau_2 = 13 \pm 1$  ps,  $\tau_3 \gg 1$  ns)

variation of the reaction conditions. Irradiation of **1** in the presence of only one equivalent of  $CO_2$  gave a new product in ~20% isolated yield (Fig. 4c). Spectroscopic and crystallographic characterization reveal the formation of the unusual, dinuclear complex [(PNP)Ni<sup>II</sup>(1 $\kappa$ C,2 $\kappa^2$ O,O'-CO<sub>2</sub>)Ni<sup>II</sup>( $\kappa^2$ P,C-tBu<sub>2</sub>PCHCHNHCHCH<sub>2</sub>PtBu<sub>2</sub>)] (**10**, Fig. 2). This product is also obtained upon photolysis of solutions of **1** and **3** under argon suggesting trapping of the photointermediate by **3** at low  $CO_2$  concentrations. The formation of **10** can be rationalized by O–H oxidative addition of **3** to a nickel(0) photoproduct and subsequent olefin migrative insertion. Initial photoinduced N–H reductive elimination to nickel(0) is further supported by a trapping experiment with CO. Photolysis under CO gives the nickel(0) complex [(CO)<sub>3</sub>Ni{ $\kappa$ P-HN(CHCHP<sub>t</sub>Bu<sub>2</sub>)<sub>2</sub>}] (**11**, Fig. 2) almost selectively (Fig. 4c). Thermal reductive elimination under CO is also observed<sup>26</sup>, yet on considerably slower timescales compared with the photolytic conditions. Reductive elimination photoreactivity is frequently observed for metal hydrides<sup>27</sup>. Surprisingly, the almost fully released pincer ligand of **11** favors the divinylamine over imine tautomer, in line with the selective transfer of the Ni–D deuteride label to the hydroxy group of **3**. In contrast, cooperative participation of the vinylic backbone, should lead to C–H/D scrambling, which is not observed<sup>22</sup>.

**Computational examinations.** This mechanistic picture was further probed by DFT computations (Fig. 5). The *trans*-NH reductive elimination product [Ni<sup>0</sup>(HPNP)] (**A**) was found at  $\Delta G = 33.2$  kcal mol<sup>-1</sup> relative to parent **1** and close to a THF solvent adduct, [(THF)Ni<sup>0</sup>(HPNP)] (**A'**,  $\Delta G = 35.9$  kcal mol<sup>-1</sup>). In contrast to the Ni<sup>II</sup> and Ni<sup>I</sup> complexes **1** and **7**, respectively, TD-DFT predicts several electronic transitions with high oscillator strength in the range 400–450 nm both for **A** and **A'** (Supplementary Fig. 40), as was found by transient UV/Vis spectroscopy (Fig. 3f). Anagostic hydrogen bonding of the amine proton indicates high basicity of the metal ion. For the unproductive oxidative addition back to parent **1**, which fully proceeds on the singlet potential energy surface, a sizable barrier ( $TS_{A/1}$ :  $\Delta G^\ddagger = 13.8$  kcal mol<sup>-1</sup>, Supplementary Fig. 45) was found that is in agreement with a persistent photoproduct on the (ps) timescale of the transient spectroscopy experiments. Carbon dioxide binding stabilizes **A** by 7.0 kcal mol<sup>-1</sup> giving side-on  $CO_2$  complex [Ni<sup>0</sup>(CO<sub>2</sub>)(HPNP)] (**B**). Alternatively, explicit solvent modeling produced intermediate [Ni<sup>0</sup>(CO<sub>2</sub>)(THF-HPNP)] (**C**) within 2.6 kcal mol<sup>-1</sup>. Anagostic N–H bonding (**B**) is in **C** replaced by a hydrogen bridge to THF. Such a structure could not be found for **A**, indicating reduced metal basicity upon binding of the  $\pi$ -acceptor  $CO_2$ . Furthermore, nitrogen is directly bound to the metal in **C** more closely resembling the {Ni(PNP)} fragment of final product **3**.



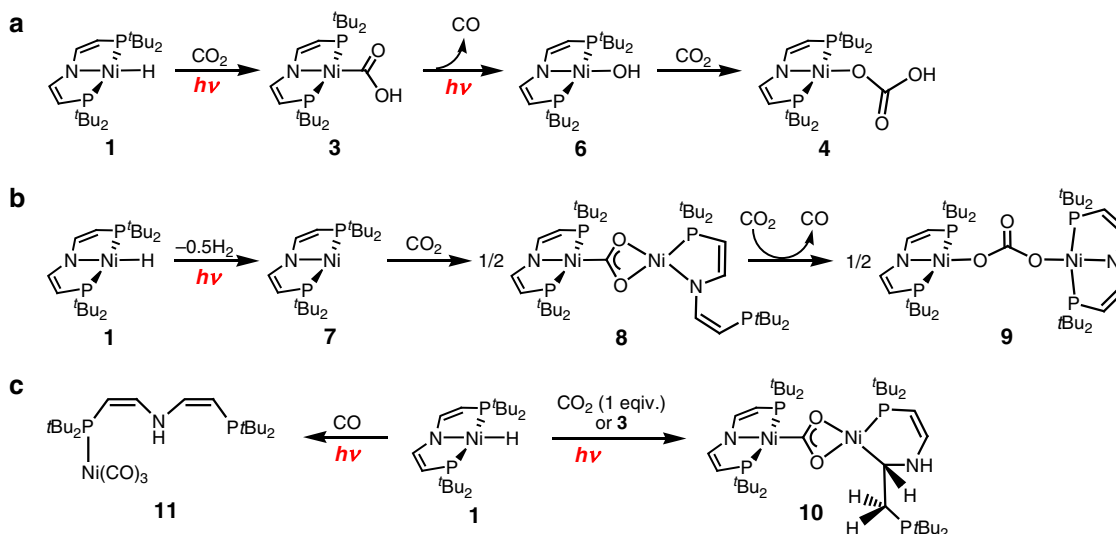


**Fig. 4** Control experiments for mechanistic rationalization. **a** Photochemical formation of hydroxycarbonate **4**. **b** Photochemical formation of nickel(I) and reaction with  $\text{CO}_2$ . **c** Photoproduct trapping experiments

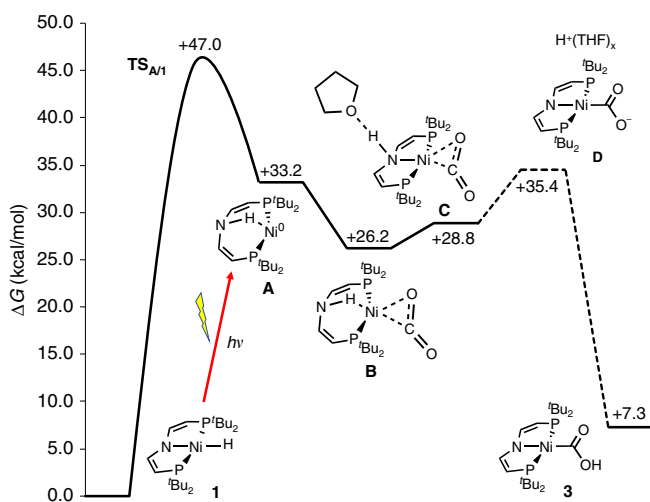


**Fig. 5** Computational examination of the proposed mechanism. Ground and transition state free energies (D3(BJ)-RI-J-PBE/def2-SVP//D3(BJ)-TPSS/def2-TZVP(Cosmo:THF)) for thermal reactivity in THF after photochemical N-H reductive elimination from **1** (red arrow). The dashed free energy for  $[\text{H}(\text{THF})_x][\text{Ni}(\text{CO}_2)(\text{PNP})]$  (**D**) ion pair formation is estimated from experimental  $\text{p}K$  derivation

This observation suggests structural flexibility of the pincer at low energetic cost. Proton coupled electron transfer to the  $\text{CO}_2$  ligand would then complete the reaction sequence. Several intra- and intermolecular routes are conceivable and were found computationally with kinetically competitive barriers below unproductive N-H oxidative addition ( $\text{TS}_{\text{A}/1}$ ). However, such values should be treated with caution without experimental benchmarking owing to the known difficulties for DFT to reliably describe proton transfer reactions with considerable charge buildup and possible direct solute-solvent interactions<sup>28</sup>. We therefore prefer to correlate intermediates **B/C** with the free energy for deprotonation of **3** in THF, which is experimentally accessible upon reaction with a reference base (Supplementary Figs. 26, 27), defining an energetic upper limit for N-to-O proton transfer. Assuming that the proton mobility is sufficient within a  $[\text{H}(\text{THF})_x\text{Ni}(\text{CO}_2)(\text{PNP})]$  (**D**) ion pair the  $\text{p}K_{\text{ip}}$  of **3** (20.6) is used, placing **D** at  $35.4 \text{ kcal mol}^{-1}$  well below  $\text{TS}_{\text{A}/1}$ , which further supports the proposed mechanism.

In summary, a mechanism that evolved from kinetic, spectroscopic, labeling, and chemical trapping experiments supported by DFT calculations explains the photochemical selectivity inversion. Photochemical excitation populates a dissociative state leading to rate-determining conversion to a photoproduct with an overall quantum yield  $\sim 5\%$ . Trapping with  $\text{CO}$ , **3** and **1**, respectively, the exclusion of nickel(I) as relevant intermediate, the retention of the Ni-D label, the photochemical timescales and the computed UV/Vis spectroscopic signatures all support the nickel(0) assignment for the immediate photoproduct as a result of intramolecular N-H reductive elimination. Hydroxycarbonyl formation presumably follows  $\text{CO}_2$  coordination to nickel(0) and proton coupled electron transfer. Hydrogen atom transfer of the photointermediate with **7** can explain the abnormal insertion rate retardation in the presence of added nickel(I) (Fig. 6).

This model implies the notion that the inversion of the  $\text{CO}_2$  insertion selectivity from normal to abnormal relies on the photochemical umpolung reaction of the hydride ligand to an N-H proton. As a consequence of this electron transfer, the reduced metal center becomes the most basic site and is subject to electrophilic attack by the substrate  $\text{CO}_2$ . This mechanistic picture therefore in several ways expresses an application of metal-ligand cooperation (MLC), which is currently extensively exploited as a strategy for catalyst design<sup>29</sup>. On one hand, photochemical transfer of the two reducing equivalents stored within the Ni-H bond to the metal presumably drives the overall endergonic abnormal  $\text{CO}_2$  insertion. On the other hand, the pincer ligand acts as a proton relay and intramolecular proton coupled electron transfer from the amine likely facilitates the  $\text{CO}_2$  two-electron reduction to the hydroxycarbonyl isomer. Hence, MLC might similarly emerge as a valuable conception for photocatalysis.

## Methods

**Synthesis and characterization.**  $[\text{Ni}\{\text{N}(\text{CHCHPr}^t\text{Bu}_2)_2\}]$  (**1**).  $[\text{NiBr}\{\text{N}(\text{CHCHPr}^t\text{Bu}_2)_2\}]$  (208 mg, 0.420 mmol, 1.00 eq) and  $\text{LiAlH}_4$  (16 mg, 0.422 mmol, 1.00 eq) are dissolved in 6 mL of THF. After stirring at room temperature for 30 mins, the solvent of the orange solution is removed in vacuo. The orange residue is extracted with pentanes and the resulting solution is filtered over Celite to yield a yellow solution. The solvent is removed in vacuo and the yellow solid is washed with  $7 \times 2 \text{ mL MeOH}$  at  $0^\circ\text{C}$ . The residue is dissolved in 10 mL of pentanes and filtered. After removal of the solvent in vacuo, the yellow solid is dissolved in a minimal amount of pentanes and recrystallized at  $-36^\circ\text{C}$ . The supernatant solution is decanted, and again recrystallized at  $-36^\circ\text{C}$ . The yellow crystalline material is dried in vacuo to yield 106 mg (0.255 mmol, 61%) of **1**. Crystals suitable for X-

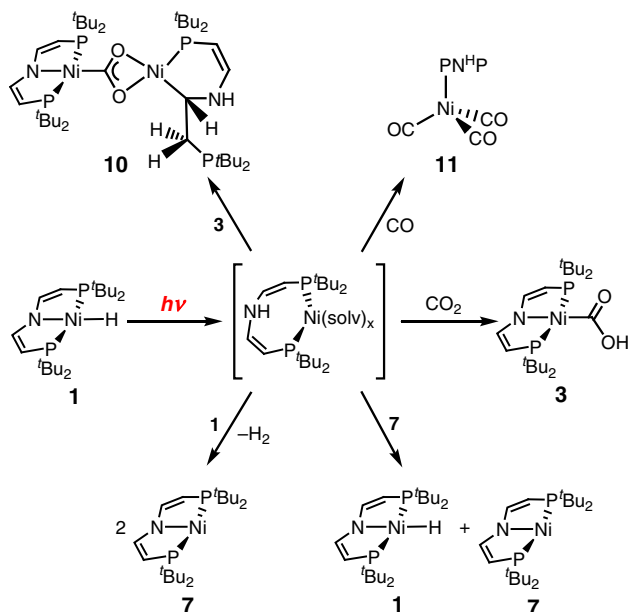


**Fig. 6** Proposed mechanism. Formation of a nickel(0) photoproduct from photochemical activation of **1** and reactivity with different substrates

ray diffraction are obtained by crystallization from pentanes at  $-36\text{ }^{\circ}\text{C}$ .  $^{31}\text{P}\{^1\text{H}\}$  NMR (121 MHz,  $\text{C}_6\text{D}_6$ )  $\delta$ : 86.2 ppm.  $^1\text{H}$  NMR (300 MHz,  $\text{C}_6\text{D}_6$ )  $\delta$ : 7.20 (ABXX'B'A',  $N = |^3J_{A-X} + ^4J_{A-X'}| = 18.3\text{ Hz}$ ,  $^3J_{A-B} = 5.0\text{ Hz}$ ,  $^4J_{H-H} = 1.9\text{ Hz}$ , 2 H, NCH), 4.09 (ABXX'B'A',  $N = |^2J_{A-X} + ^4J_{A-X'}| = 1.8\text{ Hz}$ ,  $^3J_{A-B} = 5.1\text{ Hz}$ ,  $^4J_{H-H} = 1.8\text{ Hz}$ , 2 H, PCH), (A<sub>18</sub>XX'A'<sub>18</sub>,  $N = |^3J_{A-X} + ^5J_{A-X'}| = 6.7\text{ Hz}$ , 36 H, PtBu),  $-18.52$  (tp,  $^2J_{H-P} = 59.4\text{ Hz}$ ,  $^4J_{H-H} = 2.0\text{ Hz}$ , 1 H, NiH) ppm.  $^{13}\text{C}\{^1\text{H}\}$  NMR (75 MHz,  $\text{C}_6\text{D}_6$ )  $\delta$ : 160.8 (AXX'A',  $N = |^2J_{A-X} + ^3J_{A-X'}| = 11.8\text{ Hz}$ , NCH), 83.0 (AXX'A',  $N = |^1J_{A-X} + ^3J_{A-X'}| = 15.8\text{ Hz}$ , PCH), 33.8 (A<sub>2</sub>XX'A'<sub>2</sub>,  $N = |^1J_{A-X} + ^3J_{A-X'}| = 11.1\text{ Hz}$ , PCMe<sub>3</sub>), 29.8 (A<sub>6</sub>XX'A'<sub>6</sub>,  $N = |^2J_{A-X} + ^4J_{A-X'}| = 2.9\text{ Hz}$ , PCMe<sub>3</sub>) ppm. IR (KBr):  $\tilde{\nu} = 1834.3\text{ cm}^{-1}$ . Anal. Calcd. For C<sub>40</sub>H<sub>41</sub>NNiP<sub>2</sub> (416.20): C, 57.72; H, 9.93; N, 3.37. Found: C, 57.48 H, 9.80; N, 3.41. MS (LIFDI):  $m/z$  (%) 415.1 (100).

[NiD{N(CHCHPtBu<sub>2</sub>)<sub>2</sub>}] (**1-D**). [NiBr{N(CHCHPtBu<sub>2</sub>)<sub>2</sub>}] (150 mg, 0.303 mmol, 1.00 eq) and LiAlD<sub>4</sub> (13 mg, 0.310 mmol, 1.02 eq) are dissolved in 6 mL of THF. After stirring at room temperature for 30 mins, the solvent of the orange solution is removed in vacuo. The orange residue is extracted with pentanes and the resulting solution is filtered over Celite to yield a yellow solution. The solvent is removed in vacuo and the yellow solid is washed with  $7 \times 2\text{ mL}$  MeOH at  $0\text{ }^{\circ}\text{C}$ . The residue is dissolved in 10 mL of pentanes and filtered. After removal of the solvent in vacuo, the yellow solid is dissolved in a minimal amount of pentanes and recrystallized at  $-36\text{ }^{\circ}\text{C}$ . The supernatant solution is decanted, and again recrystallized at  $-36\text{ }^{\circ}\text{C}$ . The yellow crystalline material is dried in vacuo to yield 69 mg (0.165 mmol, 55%) of **1-D**.  $^2\text{H}$  NMR (46 MHz,  $\text{C}_6\text{H}_6$ )  $\delta$ :  $-17.50$  (t,  $^2J_{H-P} = 9.0\text{ Hz}$ , NiD) ppm. IR (THF-d<sub>6</sub>):  $\tilde{\nu} = 1318, 1333\text{ cm}^{-1}$ .

[Ni(OCHO){N(CHCHPtBu<sub>2</sub>)<sub>2</sub>}] (**2**). Complex **1** (2.0 mg, 4.8  $\mu\text{mol}$ , 1.00 eq) is dissolved in 0.3 mL of THF-d<sub>8</sub> and filled into a medium wall precision pressure/vacuum valve NMR tube. The sample is degassed by three freeze–pump–thaw cycles. A total of 10 atm CO<sub>2</sub> pressure ( $\geq 99.5\%$  purity, no further purification) is applied. After 14 days, nearly complete conversion of **1** to **2** is detected.  $^{31}\text{P}\{^1\text{H}\}$  NMR (203 MHz, THF-d<sub>8</sub>)  $\delta$ : 56.1 ppm.  $^1\text{H}$  NMR (500 MHz, THF-d<sub>8</sub>)  $\delta$ : 7.25 (t,  $^4J_{H-P} = 3.4\text{ Hz}$ , 1 H, OCOH), 6.49 (ABXX'B'A',  $N = |^3J_{A-X} + ^4J_{A-X'}| = 19.1\text{ Hz}$ ,  $^3J_{A-B} = 5.5\text{ Hz}$ , 2 H, NCH), 4.09 (ABXX'B'A',  $N = |^2J_{A-X} + ^4J_{A-X'}| = 2.0\text{ Hz}$ ,  $^3J_{A-B} = 5.5\text{ Hz}$ , 2 H, PCH), 1.51 (A<sub>18</sub>XX'A'<sub>18</sub>,  $N = |^3J_{A-X} + ^5J_{A-X'}| = 6.8\text{ Hz}$ , 36 H, PtBu) ppm.  $^{13}\text{C}\{^1\text{H}\}$  NMR (126 MHz, THF-d<sub>8</sub>)  $\delta$ : 168.3 (t,  $^3J_{C-P} = 1.1\text{ Hz}$ , OCOH), 162.9 (AXX'A',  $N = |^2J_{A-X} + ^3J_{A-X'}| = 11.0\text{ Hz}$ , NCH), 83.0 (dd,  $^1J_{C-P} = 19.6\text{ Hz}$ ,  $^3J_{C-P} = 18.7\text{ Hz}$ , PCH), 35.8 (A<sub>2</sub>XX'A'<sub>2</sub>,  $N = |^1J_{A-X} + ^3J_{A-X'}| = 8.5\text{ Hz}$ , PCMe<sub>3</sub>), 29.0 (A<sub>6</sub>XX'A'<sub>6</sub>,  $N = |^2J_{A-X} + ^4J_{A-X'}| = 2.8\text{ Hz}$ , PCMe<sub>3</sub>) ppm.

[Ni(CO<sub>2</sub>H){N(CHCHPtBu<sub>2</sub>)<sub>2</sub>}] (**3**). A solution of **1** (20 mg, 0.048 mmol, 1.00 eq) in benzene (6 mL) is degassed by three pump–freeze–thaw cycles and set under 1 atm of CO<sub>2</sub> ( $\geq 99.5\%$  purity, no further purification). The reaction mixture is photolyzed ( $\lambda_{\text{exc}} > 305\text{ nm}$ ) for 8 hours, followed by washing with  $5 \times 2\text{ mL}$  of benzene and  $5 \times 2\text{ mL}$  of pentanes. The product is dissolved in THF and dried in vacuo to yield **3** (15 mg, 0.035 mmol, 73%) as a yellow solid. Crystals suitable for X-ray diffraction are obtained by diffusion of pentanes into a solution of **3** in THF.  $^{31}\text{P}\{^1\text{H}\}$  NMR (162 MHz, THF-d<sub>8</sub>)  $\delta$ : 66.2 ppm.  $^1\text{H}$  NMR (400 MHz, THF-d<sub>8</sub>)  $\delta$ : 9.51 (br, 1 H, CO<sub>2</sub>H), 6.49 (ABXX'B'A',  $N = |^3J_{A-X} + ^4J_{A-X'}| = 18.4\text{ Hz}$ ,  $^3J_{A-B} = 5.3\text{ Hz}$ , 2 H, NCH), 4.02 (ABXX'B'A',  $N = |^2J_{A-X} + ^4J_{A-X'}| = 2.0\text{ Hz}$ ,  $^3J_{A-B} = 5.2$

Hz, 2 H, PCH), 1.37 (A<sub>18</sub>XX'A'<sub>18</sub>,  $N = |^3J_{A-X} + ^5J_{A-X'}| = 6.7\text{ Hz}$ , 36 H, PtBu) ppm.  $^{13}\text{C}\{^1\text{H}\}$  NMR (126 MHz, THF-d<sub>8</sub>)  $\delta$ : 203.6 (t,  $^2J_{C-P} = 31.1\text{ Hz}$ , CO<sub>2</sub>H), 161.1 (AXX'A',  $N = |^2J_{A-X} + ^3J_{A-X'}| = 10.7\text{ Hz}$ , NCH), 82.4 (AXX'A',  $N = |^1J_{A-X} + ^3J_{A-X'}| = 18.6\text{ Hz}$ , PCH), 35.9 (A<sub>2</sub>XX'A'<sub>2</sub>,  $N = |^1J_{A-X} + ^3J_{A-X'}| = 10.2\text{ Hz}$ , PCMe<sub>3</sub>), 29.3 (A<sub>6</sub>XX'A'<sub>6</sub>,  $N = |^2J_{A-X} + ^4J_{A-X'}| = 2.7\text{ Hz}$ , PCMe<sub>3</sub>) ppm. IR (KBr):  $\tilde{\nu} = 2645, 1584, 1565\text{ cm}^{-1}$ . Anal. Calcd. For C<sub>41</sub>H<sub>41</sub>NO<sub>2</sub>NiP<sub>2</sub> (460.20): C, 54.81; H, 8.98; N, 3.04. Found: C, 54.92 H, 8.98; N, 2.91. MS (LIFDI):  $m/z$  (%) 459.0 (100).

[Ni(CO<sub>2</sub>H){N(CHCHPtBu<sub>2</sub>)<sub>2</sub>}] (**4**). A solution of [Ni(OH){N(CHCHPtBu<sub>2</sub>)<sub>2</sub>}] (**6**) in THF-d<sub>8</sub> is degassed by three pump–freeze–thaw cycles set under 1 atm CO<sub>2</sub> ( $\geq 99.9993\%$  purity, purification by passing through P<sub>4</sub>O<sub>10</sub>, Drierite and cooling to  $-40\text{ }^{\circ}\text{C}$ ) in a J-Young NMR tube. Crystals of **4** suitable for X-ray diffraction are obtained by diffusion of pentanes on a THF solution.  $^{31}\text{P}\{^1\text{H}\}$  NMR (162 MHz, THF-d<sub>8</sub>)  $\delta$ : 54.6 ppm.  $^1\text{H}$  NMR (400 MHz, THF-d<sub>8</sub>)  $\delta$ : 9.28 (br, 1 H, OCO<sub>2</sub>H), 6.47 (ABXX'B'A',  $N = |^3J_{A-X} + ^4J_{A-X'}| = 19.1\text{ Hz}$ ,  $^3J_{A-B} = 5.5\text{ Hz}$ , 2 H, NCH), 3.88 (ABXX'B'A',  $N = |^2J_{A-X} + ^4J_{A-X'}| = 2.0\text{ Hz}$ ,  $^3J_{A-B} = 5.4\text{ Hz}$ , 2 H, PCH), 1.48 (A<sub>18</sub>XX'A'<sub>18</sub>,  $N = |^3J_{A-X} + ^5J_{A-X'}| = 6.8\text{ Hz}$ , 36 H, PtBu) ppm.  $^{13}\text{C}\{^1\text{H}\}$  NMR (126 MHz, THF-d<sub>8</sub>)  $\delta$ : 163.0 (AXX'A',  $N = |^2J_{A-X} + ^3J_{A-X'}| = 11.1\text{ Hz}$ , NCH), 158.9 (s, OCO<sub>2</sub>H), 82.2 (AXX'A',  $N = |^1J_{A-X} + ^3J_{A-X'}| = 18.8\text{ Hz}$ , PCH), 35.7 (A<sub>2</sub>XX'A'<sub>2</sub>,  $N = |^1J_{A-X} + ^3J_{A-X'}| = 8.6\text{ Hz}$ , PCMe<sub>3</sub>), 29.0 (A<sub>6</sub>XX'A'<sub>6</sub>,  $N = |^2J_{A-X} + ^4J_{A-X'}| = 2.9\text{ Hz}$ , PCMe<sub>3</sub>) ppm. Evaporation of a solution of **4** results in CO<sub>2</sub> elimination and clean reformation of **6**.

[Ni(CO){N(CHCHPtBu<sub>2</sub>)<sub>2</sub>}] (**5**). A solution of [Ni{N(CHCHPtBu<sub>2</sub>)<sub>2</sub>}] (**7**) (10 mg, 0.024 mmol, 1.00 eq) in THF (0.5 mL) is degassed by three freeze–pump–thaw cycles and set under 1 atm of CO in a J-Young NMR tube. The solution is shaken at r.t. for 30 mins and the solvent is evaporated. The black residue is dissolved in pentanes and filtrated. Evaporation of the solvent and drying in vacuo gives 9 mg (0.020 mmol, 83%) of **5** as black solid. Crystals suitable for X-ray diffraction are obtained by crystallization from Et<sub>2</sub>O at  $-36\text{ }^{\circ}\text{C}$ . IR (KBr):  $\tilde{\nu} = 1910.1$  (CO)  $\text{cm}^{-1}$ . MS (LIFDI):  $m/z$  (%) 414.1 (55), 442.1 (45). For EPR characterization see Supplementary Figs. 28, 29.

[Ni(OH){N(CHCHPtBu<sub>2</sub>)<sub>2</sub>}] (**6**). [NiBr{N(CHCHPtBu<sub>2</sub>)<sub>2</sub>}] (24 mg, 0.048 mmol, 1.00 eq), KOH (30 mg, 0.535 mmol, 11.15 eq) and 15-crown-5 (10  $\mu\text{L}$ , 0.051 mmol, 1.06 eq) are filled in a J-Young NMR tube and dissolved in 1 mL THF. The solution is warmed to  $70\text{ }^{\circ}\text{C}$  for 2 days. After evaporation of the solvent, the orange solid is extracted with pentanes and filtered over celite. The solvent is evaporated and the orange powder is dissolved in pentanes and recrystallized at  $-36\text{ }^{\circ}\text{C}$ . Removal of the solvent and drying in vacuo yields red, crystalline **6** (14 mg, 0.033 mmol, 69%). Crystals suitable for X-ray diffraction are obtained by crystallization from pentanes at  $-36\text{ }^{\circ}\text{C}$ .  $^{31}\text{P}\{^1\text{H}\}$  NMR (162 MHz, THF-d<sub>8</sub>)  $\delta$ : 50.3 ppm.  $^1\text{H}$  NMR (400 MHz, THF-d<sub>8</sub>)  $\delta$ : 6.62 (ABXX'B'A',  $N = |^3J_{A-X} + ^4J_{A-X'}| = 18.8\text{ Hz}$ ,  $^3J_{A-B} = 5.4\text{ Hz}$ , 2 H, NCH), 3.88 (ABXX'B'A',  $N = |^2J_{A-X} + ^4J_{A-X'}| = 1.9\text{ Hz}$ ,  $^3J_{A-B} = 5.3\text{ Hz}$ , 2 H, PCH), 1.37 (A<sub>18</sub>XX'A'<sub>18</sub>,  $N = |^3J_{A-X} + ^5J_{A-X'}| = 6.6\text{ Hz}$ , 36 H, PtBu),  $-4.88$  (t,  $^3J_{H-P} = 5.6\text{ Hz}$ , OH) ppm.  $^{13}\text{C}\{^1\text{H}\}$  NMR (126 MHz, THF-d<sub>8</sub>)  $\delta$ : 162.8 (AXX'A',  $N = |^2J_{A-X} + ^3J_{A-X'}| = 11.8\text{ Hz}$ , NCH), 81.2 (AXX'A',  $N = |^1J_{A-X} + ^3J_{A-X'}| = 18.3\text{ Hz}$ , PCH), 35.2 (A<sub>2</sub>XX'A'<sub>2</sub>,  $N = |^1J_{A-X} + ^3J_{A-X'}| = 8.6\text{ Hz}$ , PCMe<sub>3</sub>), 29.3 (A<sub>6</sub>XX'A'<sub>6</sub>,  $N = |^2J_{A-X} + ^4J_{A-X'}| = 2.9\text{ Hz}$ , PCMe<sub>3</sub>) ppm. IR (Nujol):  $\tilde{\nu} = 3643.8\text{ cm}^{-1}$ . Anal. Calcd. For C<sub>40</sub>H<sub>41</sub>NO<sub>2</sub>NiP<sub>2</sub> (416.20): C, 55.58; H, 9.56; N, 3.24. Found: C, 55.50 H, 9.46; N, 3.12. MS (LIFDI):  $m/z$  (%) 431.2 (100).

[Ni{N(CHCHPtBu<sub>2</sub>)<sub>2</sub>}] (**7**). [NiBr{N(CHCHPtBu<sub>2</sub>)<sub>2</sub>}] (80 mg, 0.162 mmol, 1.00 eq) and magnesium powder (78 mg, 3.21 mmol, 19.8 eq) are suspended in 5 mL THF and stirred for 30 mins at room temperature accompanied by a color change to orange. The solvent is evaporated, and the residue is dissolved in pentanes and filtered over celite. The solution is dried in vacuo and the orange powder is dissolved in a minimal amount of pentanes and recrystallized at  $-36\text{ }^{\circ}\text{C}$ . The mother liquor is decanted after 3 days and this procedure is repeated two times, giving 42 mg (0.101 mmol, 62%) of **7** as orange crystals. Crystals suitable for X-ray diffraction are obtained by crystallization from pentanes at  $-36\text{ }^{\circ}\text{C}$ .  $^1\text{H}$  NMR (400 MHz,  $\text{C}_6\text{D}_6$ )  $\delta$ : 7 (br, tBu),  $-62$  (br, CH) ppm. Anal. Calcd. For C<sub>20</sub>H<sub>40</sub>NP<sub>2</sub>Ni (415.19): C, 57.86; H, 9.71; N, 3.37. Found: C, 57.59 H, 9.48; N, 3.27. MS (LIFDI):  $m/z$  (%) 414.1 (100).

[[N(CHCHPtBu<sub>2</sub>)<sub>2</sub>]<sub>2</sub>Ni(1κC,2κ<sup>2</sup>O, O<sup>-13</sup>CO<sub>2</sub>)Ni(κ<sup>2</sup>P,N-N(CHCHPtBu<sub>2</sub>)<sub>2</sub>)] (**8**). Complex **7** (5.0 mg, 0.012 mmol, 1.00 eq) is dissolved in 0.5 mL  $\text{C}_6\text{D}_6$  in a J-Young NMR tube and 300  $\mu\text{L}$  (0.012 mmol, 1.00 eq) <sup>13</sup>CO<sub>2</sub> are added with a syringe. The solution is kept at room temperature for 24 h.  $^{31}\text{P}\{^1\text{H}\}$  NMR (162 MHz,  $\text{C}_6\text{D}_6$ )  $\delta$ : 72.2 (dd,  $^5J_{P-P} = 8.7\text{ Hz}$ ,  $^3J_{P-C} = 2.4\text{ Hz}$ , 1 P, (PNP)NiCO<sub>2</sub>Ni(PN)), 67.8 (d,  $^2J_{P-C} = 29.1\text{ Hz}$ , 2 P, (PNP)NiCO<sub>2</sub>Ni(PN)), 4.77 (d,  $^5J_{P-P} = 8.6\text{ Hz}$ , 1 P, non-coordinating pincer arm) ppm.  $^1\text{H}$  NMR (400 MHz,  $\text{C}_6\text{D}_6$ )  $\delta$ : 8.23 (ddd,  $^3J_{H-P} = 42.4\text{ Hz}$ ,  $^4J_{H-P} = 5.5\text{ Hz}$ ,  $^3J_{H-H} = 5.5\text{ Hz}$ , 1 H, NCH non-coordinating pincer arm), 6.86 (ABXX'B'A',  $N = |^3J_{A-X} + ^4J_{A-X'}| = 18.4\text{ Hz}$ ,  $^3J_{A-B} = 5.2\text{ Hz}$ , 2 H, NCH), 6.43 (ddd,  $^3J_{H-P} = 20.8\text{ Hz}$ ,  $^2J_{H-H} = 10.5\text{ Hz}$ , 1 H, NCH coordinating pincer arm), 4.69 (dd,  $^2J_{H-H} = 10.5\text{ Hz}$ ,  $^2J_{H-P} = 6.4\text{ Hz}$ , 1 H, PCH coordinating pincer arm), 3.95 (m, 2 H, PCH), 3.40 (dd,  $^2J_{H-P} = 4.8\text{ Hz}$ ,  $^2J_{H-H} = 4.8\text{ Hz}$ , 1 H, PCH non-coordinating pincer arm), 1.60 (m, 36 H, PtBu), 1.47 (d,  $^3J_{H-P} = 13.6\text{ Hz}$ , 18 H, PtBu coordinating pincer arm), 1.25 (d,  $^3J_{H-P} = 10.9\text{ Hz}$ , 18 H, PtBu non-coordinating pincer arm) ppm.  $^{13}\text{C}\{^1\text{H}\}$  NMR (101 MHz,  $\text{C}_6\text{D}_6$ )  $\delta$ : 236.7 (t,  $^2J_{C-P} = 29.1\text{ Hz}$ ,  $^3J_{C-P} = 2.4\text{ Hz}$ , CO<sub>2</sub>), 165.8 (dd,  $^2J_{C-P} = 23.0\text{ Hz}$ ,  $^3J_{C-P} = 13.7\text{ Hz}$ , NCH non-coordinating pincer arm), 160.9 (AXX'A',  $N = |^2J_{A-X} + ^3J_{A-X'}| = 10.4\text{ Hz}$ , NCH), 149.8 (d,  $^2J_{C-P} = 14.1\text{ Hz}$ , NCH), 96.4 (d,  $^1J_{C-P} = 18.8\text{ Hz}$ , PCH), 82.3 (AXX'A',  $N = |^1J_{A-X} + ^3J_{A-X'}| = 18.6\text{ Hz}$ , PCH), 74.9 (d,  $^1J_{P-C} = 47.5$ , PCH non-coordinating pincer arm), 36.0 (A<sub>2</sub>XX'A'<sub>2</sub>,  $N = |^1J_{A-X} + ^3J_{A-X'}| = 10.3\text{ Hz}$ , PCMe<sub>3</sub>), 35.0 (d,  $^1J_{C-P} = 20.9\text{ Hz}$ , PCMe<sub>3</sub>), 32.4 (d,  $^1J_{C-P} = 19.5\text{ Hz}$ , PCMe<sub>3</sub>), 30.0 (d,  $^2J_{C-P} = 14.3\text{ Hz}$ , PCMe<sub>3</sub>), 29.7 (br, PCMe<sub>3</sub>), 28.9

(d,  $^1J_{C-P} = 4.1$  Hz, PCMe<sub>3</sub>), 30.0 (d,  $^2J_{C-P} = 14.3$  Hz, PCMe<sub>3</sub>) ppm. Assignment of signals is based on selectively decoupled  $^1H\{^31P\}$  and 2D NMR spectra. MS (LIFDI):  $m/z$  (%) 872.3 (100).

$\{[Ni(CHCHP(Bu_2)_2)]Ni(OC(O)O)Ni\{[Ni(CHCHP(Bu_2)_2)]\}$  (9). Complex 7 (3.2 mg, 0.008 mmol, 1.00 eq) and 3  $\mu$ L O(SiMe<sub>3</sub>)<sub>2</sub> as internal standard are dissolved in 0.5 mL THF-d<sub>8</sub>. The solution is degassed by three pump-freeze-thaw cycles and 1 atm CO<sub>2</sub> ( $\geq 99.9993\%$  purity, purification by passing through P<sub>4</sub>O<sub>10</sub>, Drierite and cooling to  $-40^\circ$ C) is applied. The solution is stirred at room temperature for 11 days. Crystals suitable for X-ray diffraction are obtained by crystallization from pentanes at  $-36^\circ$ C.  $^31P\{^1H\}$  NMR (162 MHz, THF-d<sub>8</sub>)  $\delta$ : 49.2 ppm.  $^1H$  NMR (400 MHz, THF-d<sub>8</sub>)  $\delta$ : 6.31 (ABXX'B'A',  $N = |^3J_{A-X} + ^4J_{A-X'}| = 17.9$  Hz,  $^3J_{A-B} = 5.6$  Hz, 4 H, NCH), 3.80 (d,  $^3J_{H-H} = 5.6$  Hz, 4 H, PCH), 1.50 (A<sub>18</sub>XX'A'<sub>18</sub>,  $N = |^3J_{A-X} + ^5J_{A-X'}| = 6.7$  Hz, 72 H, PtBu), ppm.  $^{13}C\{^1H\}$  NMR (126 MHz, C<sub>6</sub>D<sub>6</sub>)  $\delta$ : 162.5 (s, OC(O)O) ppm. MS (LIFDI):  $m/z$  (%) 889.3 (100,  $^{13}CO_3^{2-}$ -isotopologue).

$\{[Ni(CHCHP(Bu_2)_2)]Ni(\kappa C,2 \kappa^2 O, O^--CO_2)Ni\{\kappa^2 P, C-tBu_2PCHCHNHCCH_2, PtBu_2\}\}$  (10). Synthesis from 1 and CO<sub>2</sub>: Complex 1 (30 mg, 0.072 mmol, 1.00 eq) is dissolved in 3 mL benzene and 1.8 mL CO<sub>2</sub> (0.074 mmol, 1.03 eq,  $\geq 99.9993\%$  purity, purification by passing through P<sub>4</sub>O<sub>10</sub>, Drierite and cooling to  $-40^\circ$ C) are added by syringe. The solution is photolyzed ( $\lambda_{exc} > 305$  nm) over night and the solvent is evaporated. The residue is dissolved in pentanes, filtered, and the solvent is evaporated. The residue is suspended in 1 mL acetonitrile and diethyl ether is added dropwise until the solid is dissolved completely. Repeated crystallization at  $-36^\circ$ C and subsequent drying in vacuo gives orange 10 (7 mg, 0.008 mmol, 22%). Crystals suitable for X-ray diffraction are obtained by crystallization from pentanes at  $-36^\circ$ C. Synthesis from 1 and 3: 3 (1.5 mg, 3.3  $\mu$ mol, 1.00 eq) and 1 (1.4 mg, 3.4  $\mu$ mol, 1.03 eq) are dissolved in 0.5 mL THF and filled in a J-Young NMR tube and the sample is photolyzed ( $\lambda_{exc} > 305$  nm).  $^31P\{^1H\}$  NMR (203 MHz, C<sub>6</sub>D<sub>6</sub>)  $\delta$ : 66.2 (d,  $^2J_{P-P} = 197.3$  Hz, 1 P, (PNP)NiCO<sub>2</sub>Ni(PC)), 65.0 (d,  $^2J_{P-P} = 197.1$  Hz, 1 P, (PNP)NiCO<sub>2</sub>Ni(PC)), 36.8 (d,  $^4J_{P-P} = 7.4$  Hz, 1 P, (PNP)NiCO<sub>2</sub>Ni(PC)), 17.1 (d,  $^4J_{P-P} = 7.2$  Hz, 1 P, non-coordinating pincer arm) ppm.  $^1H$  NMR (500 MHz, C<sub>6</sub>D<sub>6</sub>)  $\delta$ : 6.96 (m, 2 H, NCH), 6.48 (ddd,  $^2J_{H-P} = 27.2$  Hz,  $^3J_{H-H} = 9.6$  Hz,  $^4J_{H-H} = 7.5$  Hz, 1 H, PCH), 4.37 (dd,  $^4J_{H-P} = 7.4$  Hz,  $^4J_{H-H} = 7.4$  Hz, 1 H, NH), 4.02 (m, 2 H, PCH), 3.52 (d,  $^3J_{H-H} = 9.6$  Hz, 1 H, NCH), 2.92 (dddd,  $^3J_{H-H} = 12.4$  Hz,  $^3J_{H-P} = 6.1$  Hz,  $^3J_{H-H} = 1.9$  Hz,  $^3J_{H-H} = 1.9$  Hz, 1 H, NCHCH<sub>2</sub>), 2.72 (ddd,  $^2J_{H-H} = 14.3$  Hz,  $^2J_{H-P} = 5.9$  Hz,  $^3J_{H-H} = 2.1$  Hz, 1 H, NCHCHH), 1.73 (m, 9 H, PtBu), 1.68 (m, 9 H, PtBu), 1.59 (m, 9 H, PtBu), 1.51 (m, 9 H, PtBu), 1.50 (d,  $^3J_{H-P} = 12.9$  Hz, 9 H, PtBu), 1.47 (d,  $^3J_{H-P} = 13.1$  Hz, 9 H, PtBu), 1.47 (NCHCHH, detected by  $^1H\{^1H$  COSY NMR), 1.32 (d,  $^3J_{H-P} = 10.7$  Hz, 9 H, PtBu), 1.19 (d,  $^3J_{H-P} = 10.9$  Hz, 9 H, PtBu) ppm.  $^{13}C\{^1H\}$  NMR (126 MHz, C<sub>6</sub>D<sub>6</sub>)  $\delta$ : 228.3 (dt,  $^2J_{C-P} = 28.5$  Hz,  $^3J_{C-P} = 3.0$  Hz, NiCO<sub>2</sub>Ni), 160.7 (dd,  $^3J_{C-P} = 13.9$  Hz,  $^2J_{C-P} = 7.3$  Hz, NCH), 160.7 (dd,  $^3J_{C-P} = 14.0$  Hz,  $^2J_{C-P} = 7.1$  Hz, NCH), 149.0 (d,  $^2J_{C-P} = 7.3$  Hz, NCH), 82.6 (dd,  $^1J_{C-P} = 33.3$  Hz,  $^3J_{C-P} = 9.4$  Hz, PCH), 82.4 (dd,  $^1J_{C-P} = 32.5$  Hz,  $^3J_{C-P} = 9.5$  Hz, PCH), 68.0 (dd,  $^1J_{C-P} = 50.7$  Hz, PCH), 36.2 (dd,  $^1J_{C-P} = 13.8$ ,  $^3J_{C-P} = 6.0$  Hz, PCMe<sub>3</sub>), 35.9 (dd,  $^1J_{C-P} = 14.0$ ,  $^3J_{C-P} = 5.8$  Hz, PCMe<sub>3</sub>), 35.8 (dd,  $^1J_{C-P} = 14.2$ ,  $^3J_{C-P} = 6.0$  Hz, PCMe<sub>3</sub>), 35.4 (dd,  $^1J_{C-P} = 14.2$ ,  $^3J_{C-P} = 6.4$  Hz, PCMe<sub>3</sub>), 35.0 (d,  $^1J_{C-P} = 21.4$ , PCMe<sub>3</sub>), 34.6 (d,  $^1J_{C-P} = 24.4$ , PCMe<sub>3</sub>), 33.2 (dd,  $^2J_{C-P} = 30.4$  Hz,  $^2J_{C-P} = 4.1$  Hz, NCHNi), 32.6 (d,  $^1J_{C-P} = 22.9$  Hz, PCMe<sub>3</sub>), 31.2 (d,  $^1J_{C-P} = 21.6$  Hz, PCMe<sub>3</sub>), 30.5 (d,  $^2J_{C-P} = 12.7$  Hz, PCMe<sub>3</sub>), 30.2 (dd,  $^2J_{C-P} = 3.9$  Hz,  $^4J_{C-P} = 1.8$  Hz, PCMe<sub>3</sub>), 30.1 (dd,  $^2J_{C-P} = 3.8$  Hz,  $^4J_{C-P} = 1.8$  Hz, PCMe<sub>3</sub>), 39.9 (d,  $^1J_{C-P} = 13.3$  Hz, PCMe<sub>3</sub>), 29.7 (d,  $^2J_{C-P} = 5.0$  Hz, 2xPCMe<sub>3</sub>), 29.7 (dd,  $^2J_{C-P} = 3.7$  Hz,  $^4J_{C-P} = 1.8$  Hz, PCMe<sub>3</sub>), 29.6 (dd,  $^2J_{C-P} = 3.7$  Hz,  $^4J_{C-P} = 1.6$  Hz, PCMe<sub>3</sub>), 29.4 (d,  $^1J_{C-P} = 26.9$  Hz, CH<sub>2</sub>) ppm. IR (THF-d<sub>8</sub>):  $\tilde{\nu} = 1526.4, 1611.3, 3333.5$  cm<sup>-1</sup>. MS (LIFDI):  $m/z$  (%) 873.4 (50), 1392.5 (50).

$\{[CO_2]Ni\{\kappa^2 P-HN(CHCHP(Bu_2)_2)\}\}$  (11). A solution of 1 (9.69 mmol, 0.5 mL) in THF-d<sub>8</sub> and O(SiMe<sub>3</sub>)<sub>2</sub> as internal standard are filled into a J-Young NMR tube, degassed by three pump-freeze-thaw cycles and 1 atm of CO applied. The sample is photolyzed ( $\lambda_{exc} > 305$  nm) for 90 minutes. Crystals of 11 suitable for X-ray diffraction are obtained by crystallization from acetonitrile at  $-36^\circ$ C.  $^31P\{^1H\}$  NMR (162 MHz, THF-d<sub>8</sub>)  $\delta$ : 39.3 (PNI(CO)<sub>3</sub>),  $-5.2$  ppm.  $^1H$  NMR (400 MHz, THF-d<sub>8</sub>)  $\delta$ : 8.10 (dd,  $^3J_{H-H} = 12.3$  Hz,  $^3J_{H-H} = 12.3$  Hz, 1 H, NH), 6.92 (dddd,  $^3J_{H-P} = 24.8$  Hz,  $^3J_{H-H} = 13.0$  Hz,  $^3J_{H-H} = 10.8$  Hz,  $^4J_{H-H} = 2.4$  Hz, 1 H, NCHCHPNI(CO)<sub>3</sub>), 6.88 (ddd,  $^3J_{H-P} = 18.1$  Hz,  $^3J_{H-H} = 11.6$  Hz,  $^3J_{H-H} = 9.5$  Hz, 1 H, NCH), 4.74 (dd,  $^3J_{H-H} = 9.5$  Hz,  $^2J_{H-P} = 4.8$  Hz, 1 H, PCH), 4.46 (dd,  $^3J_{H-H} = 10.7$  Hz,  $^2J_{H-P} = 2.4$  Hz, 1 H, HCPNI(CO)<sub>3</sub>), 1.24 (d,  $^3J_{H-P} = 13.3$  Hz, 18 H, tBu<sub>2</sub>PNI(CO)<sub>3</sub>), 1.23 (d,  $^3J_{H-P} = 12.3$  Hz, 18 H, PtBu<sub>2</sub>) ppm.  $^{13}C\{^1H\}$  NMR (101 MHz, THF-d<sub>8</sub>)  $\delta$ : 198.5 (d,  $^2J_{C-P} = 3.8$  Hz, Ni(CO)<sub>3</sub>), 145.5 (d,  $^2J_{C-P} = 5.8$  Hz, NCH), 145.0 (d,  $^2J_{C-P} = 20.4$  Hz, NCH), 95.3 (d,  $^1J_{C-P} = 17.1$  Hz, PCH), 84.9 (d,  $^1J_{C-P} = 30.7$  Hz, PCH), 35.9 (d,  $^1J_{C-P} = 35.9$  Hz, PCMe<sub>3</sub>), 31.9 (d,  $^1J_{C-P} = 16.3$  Hz, PCMe<sub>3</sub>), 29.7 (d,  $^2J_{C-P} = 13.8$  Hz, PCMe<sub>3</sub>), 29.2 (d,  $^2J_{C-P} = 7.1$  Hz, PCMe<sub>3</sub>) ppm. IR (Nujol):  $\tilde{\nu} = 3316.5, 2062.7, 1987.9$  cm<sup>-1</sup>. MS (LIFDI):  $m/z$  (%) 443.4 (100). Evaporation in vacuo results in CO loss and reformation of 1.

**Data availability.** Detailed descriptions of experimental and spectroscopic methods and results are available within this paper and its supplementary information files. For NMR spectra of the compounds in this article, see Supplementary Figs 1–14. For quantum chemical methods and results see Supplementary Figs 38–47 and Supplementary Tables 1–18. The crystallographic data CCDC-1561988–1561994, CCDC-1574302, and CCDC-1574303 can be obtained free of charge from the Cambridge Crystallographic Data Centre ([www.ccdc.cam.ac.uk/data\\_request/cif](http://www.ccdc.cam.ac.uk/data_request/cif)). All other data are available from the authors upon reasonable request.

Received: 3 October 2017 Accepted: 29 January 2018

Published online: 21 March 2018

## References

- Appel, A. M. et al. Frontiers, opportunities, and challenges in biochemical and chemical catalysis of CO<sub>2</sub> fixation. *Chem. Rev.* **113**, 6621–6658 (2013).
- Volbeda, A. & Fontecilla-Camps, J. C. Structural bases for the catalytic mechanism of Ni-containing carbon monoxide dehydrogenases. *Dalton Trans.* 3443–3450 (2005).
- Hammouche, M. et al. Chemical catalysis of electrochemical reactions. Homogeneous catalysis of the electrochemical reduction of carbon dioxide by iron(0) porphyrins. Role of the addition of magnesium cations. *J. Am. Chem. Soc.* **113**, 8455–8466 (1991).
- Fujita, E., Furenli, L. R. & Renner, M. W. Direct XANES evidence for charge transfer in Co-CO<sub>2</sub> complexes. *J. Am. Chem. Soc.* **119**, 4549–4550 (1997).
- Feller, M. et al. Reductive cleavage of CO<sub>2</sub> by metal-ligand-cooperation mediated by an iridium pincer complex. *J. Am. Chem. Soc.* **138**, 6445–6454 (2016).
- Sato, S., Morikawa, T., Kajino, T. & Ishitani, O. A highly efficient mononuclear iridium complex photocatalyst for CO<sub>2</sub> reduction under visible light. *Angew. Chem. Int. Ed.* **52**, 988–992 (2013).
- Garg, K. et al. Striking differences in properties of geometric isomers of [Ir(tpy)-(ppy)H]<sup>+</sup>: experimental and computational studies of their hydricities, interaction with CO<sub>2</sub>, and photochemistry. *Angew. Chem. Int. Ed.* **54**, 14128–14132 (2015).
- Bourrez, M. et al. Pulsed-EPR evidence of a manganese(II) hydroxycarbonyl intermediate in the electrocatalytic reduction of carbon dioxide by a manganese bipyridyl derivative. *Angew. Chem. Int. Ed.* **126**, 240–243 (2014).
- Rakowski DuBois, M. & DuBois, D. L. Development of molecular electrocatalysts for CO<sub>2</sub> reduction and H<sub>2</sub> production/oxidation. *Acc. Chem. Res.* **42**, 1974–1982 (2009).
- Schneider, J., Jia, H., Muckerman, J. T. & Fujita, E. Thermodynamics and kinetics of CO<sub>2</sub>, CO, and H<sup>+</sup> binding to the metal centre of CO<sub>2</sub> reduction catalysts. *Chem. Soc. Rev.* **41**, 2036–2051 (2012).
- Constantin, C., M. Robert, M. & Savéant, J.-M. Current issues in molecular catalysis illustrated by iron porphyrins as catalysts of the CO<sub>2</sub>-to-CO electrochemical conversion. *Acc. Chem. Res.* **48**, 2996–3006 (2015).
- Berardi, S. et al. Molecular artificial photosynthesis. *Chem. Soc. Rev.* **43**, 7501–7519 (2014).
- Jessop, P. G., Ikariya, T. & Noyori, R. Homogeneous hydrogenation of carbon dioxide. *Chem. Rev.* **95**, 259–272 (1995).
- Jessop, P. G., Joo, F. & Tai, C.-C. Recent advances in the homogeneous hydrogenation of carbon dioxide. *Coord. Chem. Rev.* **248**, 2425–2442 (2004).
- Wang, W.-H., Himeda, Y., Muckerman, J. T., Manbeck, G. F. & Fujita, E. CO<sub>2</sub> hydrogenation to formate and methanol as an alternative to photo- and electrochemical CO<sub>2</sub> reduction. *Chem. Rev.* **115**, 12936–12973 (2015).
- Alberico, E. & Nielsen, M. Towards a methanol economy based on homogeneous catalysis: methanol to H<sub>2</sub> and CO<sub>2</sub> to methanol. *Chem. Commun.* **51**, 6714–6725 (2015).
- Fan, T., Chen, X. & Lin, Z. Theoretical studies of reactions of carbon dioxide mediated and catalysed by transition metal complexes. *Chem. Commun.* **48**, 10808–10828 (2012).
- Yoo, C., Kim, J. & Lee, Y. Synthesis and reactivity of nickel(II) hydroxycarbonyl species, NiCOOH- $\kappa$ C. *Organometallics* **32**, 7195–7203 (2013).
- Yoo, C. & Lee, Y. Carbon dioxide binding at a Ni/Fe center: synthesis and characterization of Ni( $\eta^1$ -CO<sub>2</sub>- $\kappa$ C) and Ni- $\mu$ -CO<sub>2</sub>- $\kappa$ C: $\kappa^2$ O'-Fe. *Chem. Sci.* **8**, 600–605 (2017).
- Yoo, C. & Lee, Y. A T-shaped nickel(I) metalloradical species. *Angew. Chem. Int. Ed.* **56**, 9502–9506 (2017).
- Chakraborty, S., Bhattacharya, P., Dai, H. & Guan, H. Nickel and iron pincer complexes as catalysts for the reduction of carbonyl compounds. *Acc. Chem. Res.* **48**, 1995–2003 (2015).
- Schneck, F., Finger, M., Tromp, M. & Schneider, S. Chemical non-innocence of an aliphatic PNP pincer ligand. *Chem. Eur. J.* **23**, 33–37 (2017).
- Zimmermann, P. & Limberg, C. Activation of small molecules at nickel(I) moieties. *J. Am. Chem. Soc.* **139**, 4233–4242 (2017).
- Ingleson, M. J. et al. Influence of the d-electron count on CO binding by three-coordinate [(tBu<sub>2</sub>PCH<sub>2</sub>SiMe<sub>2</sub>)<sub>2</sub>N]Fe, -Co, and -Ni. *Inorg. Chem.* **47**, 407–409 (2008).
- Rettenmeier, C., Wade, H. & Gade, L. H. Electronic structure and reactivity of nickel(I) pincer complexes: their aerobic transformation to peroxo species and site selective C–H oxygenation. *Chem. Sci.* **7**, 3533–3542 (2016).
- Liang, L.-C. et al. Divergent carbonylation reactivity preferences of nickel complexes containing amido pincer ligands: migratory insertion versus reductive elimination. *Organometallics* **31**, 700–708 (2012).

27. Perutz, R. N. & Procacci, B. Photochemistry of transition metal hydrides. *Chem. Rev.* **116**, 8506–8544 (2016).
28. Ho, J. & Coote, M. L. A universal approach for continuum solvent  $pK_a$  calculations: are we there yet? *Theor. Chem. Acc.* **125**, 3–21 (2010).
29. Khusnutdinova, J. R. & Milstein, D. Metal-ligand cooperation. *Angew. Chem. Int. Ed.* **54**, 12236–12273 (2015).

### Acknowledgements

This work was supported by grants from the European Research Council (ERC Grant Agreement 646747) and the Deutsche Forschungsgemeinschaft (CRC 1073, Project C07).

### Author contributions

F.S. planned and performed all synthetic work and characterization (except transient spectroscopy) supervised by S.S. A.C.S. assisted the EPR spectroscopic examinations and C.W. the crystallographic characterizations. M.F. carried out the quantum chemical study. J.A. carried out the transient spectroscopy experiments supervised by D.S. The paper was co-written by F.S. and S.S. and all authors discussed the results and commented on the manuscript.

### Additional information

**Supplementary Information** accompanies this paper at <https://doi.org/10.1038/s41467-018-03239-3>.

**Competing interests:** The authors declare no competing financial interests.

**Reprints and permission** information is available online at <http://npg.nature.com/reprintsandpermissions/>

**Publisher's note:** Springer Nature remains neutral with regard to jurisdictional claims in published maps and institutional affiliations.



**Open Access** This article is licensed under a Creative Commons Attribution 4.0 International License, which permits use, sharing, adaptation, distribution and reproduction in any medium or format, as long as you give appropriate credit to the original author(s) and the source, provide a link to the Creative Commons license, and indicate if changes were made. The images or other third party material in this article are included in the article's Creative Commons license, unless indicated otherwise in a credit line to the material. If material is not included in the article's Creative Commons license and your intended use is not permitted by statutory regulation or exceeds the permitted use, you will need to obtain permission directly from the copyright holder. To view a copy of this license, visit <http://creativecommons.org/licenses/by/4.0/>.

© The Author(s) 2018